frontiers | Frontiers in Energy Research

TYPE Original Research
PUBLISHED 29 August 2022
DOI 10.3389/fenrg.2022.883206

OPEN ACCESS

EDITED BY
Qingsong Wang,
University of Bayreuth, Germany

REVIEWED BY
Keke Chang,
Ningbo Institute of Materials Technology and Engineering (CAS), China
Yan Lu,
Shandong University, China
Li Wenwu,
Sungkyunkwan University, South Korea

*CORRESPONDENCE
P. Ghigna,
paolo.ghigna@unipv.it

SPECIALTY SECTION
This article was submitted to Electrochemical Energy Conversion and Storage,
a section of the journal
Frontiers in Energy Research

RECEIVED 24 February 2022
ACCEPTED 05 July 2022
PUBLISHED 29 August 2022

CITATION
Fracchia M, Callegari D, Coduri M, Anselmi-Tamburini U, Manzoli M, Quartarone E and Ghigna P (2022), Electrochemical performance of high and medium entropy oxides for lithium batteries.
Front. Energy Res. 10:883206.
doi: 10.3389/fenrg.2022.883206

Electrochemical performance of high and medium entropy oxides for lithium batteries

M. Fracchia[1,2], D. Callegari[1], M. Coduri[1,2], U. Anselmi-Tamburini[1,2], M. Manzoli[3], E. Quartarone[1] and P. Ghigna[1,2]*

[1]Department of Chemistry, University of Pavia, Pavia, Italy, [2]INSTM, National Inter-University Consortium for Materials Science and Technology, Florence, Italy, [3]Department of Drug Science and Technology and NIS—Centre for Nanostructured Interfaces and Surfaces, Turin, Italy

Various high and medium entropy oxides with rock salt structures were prepared and studied as anodes for lithium batteries. All the systems had complex reaction mechanisms involving conversion reactions. Their capacity and reduction potential depend on the number of components and microstructure of the initial materials. However, the dependence is difficult to rationalize based on simple stability logic. This paper discusses the implication of our findings in the wider context of the science of high entropy materials.

KEYWORDS

high entropy oxides, middle entropy oxides, lithium batteries, conversion reaction, anodes, irreversibility

Introduction

The recent discovery of $Mg_{0.2}Co_{0.2}Ni_{0.2}Cu_{0.2}Zn_{0.2}O$ by Rost et al. (Rost et al., 2015) has led to a flourishing of research in the field of high entropy oxides (HEOs). These are a class of ceramic materials with several crystal structures (rock-salt (Rost et al., 2015; Yan et al., 2018), fluorite (Gild et al., 2018; Spiridigliozzi et al., 2021), spinel (Dąbrowa et al., 2018; Fracchia et al., 2020b; Mao et al., 2020), and perovskite (Sarkar et al., 2018a; Jiang et al., 2018; Vinnik et al., 2020), etc.) where the presence of several parent oxides forming a solid solution gives rise to a high value in the configurational entropy of the system, which can be expressed as:

$$S_{config} = -R\sum_i^n x_i \ln x_i$$

The configurational entropy, particularly large in the presence of multiple components, enters as a stabilizing factor in the Gibbs free energy of formation of these compounds and is thought to be a fundamental term in the formation of single-phase solid solutions, compensating for possible unfavorable enthalpic contributions. The example of $Mg_{0.2}Co_{0.2}Ni_{0.2}Cu_{0.2}Zn_{0.2}O$ is retained as paradigmatic, as this compound adopts a rock-salt crystal structure. While the parent oxides NiO, CoO and MgO do have

the same crystal structure, CuO and ZnO do not; the high configurational entropy (S_{config}) of the resulting solid solution is usually accepted as the main stabilizing term in Gibbs free energy. However, this rationale was recently questioned by Fracchia *et al.* on the basis of copper oxide containing solid solutions with the rock-salt structure also forming in less-than-five component systems, where the role of configurational entropy is significantly lower (Fracchia, 2022). Analogously to high entropy alloys (Tsai et al., 2014; Miracle and Senkov, 2017; George et al., 2019), the high entropy stabilization rationale requires that the compositional space is randomly sampled. This is hardly the case for HEOs: in fact, three out of the five components are stable in the rock salt structure, while the solubility of ZnO and CuO in a cubic rock-salt binary oxide is close to 20% (molar ratio) (Navrotsky and Muan, 1971; Davies, 1982; Bulazirk et al., 1986; Zabdyr and Fabrichnaya, 2002), which is the molar fraction employed in this case. The compositional bias is particularly evident for HEOs with a spinel structure, where the parent oxides are, in almost all cases, not randomly selected but are instead spinel-forming materials (Dąbrowa et al., 2018; Fracchia et al., 2020b; Chen et al., 2020; Stygar et al., 2020). In this case, at the temperatures used for the synthesis, the Gibbs free energy of formation is always negative and large but is, in most cases, nearly one order of magnitude larger (in absolute value) than the stabilizing term given by configurational entropy. Therefore, the crystal field stabilization energy seems to be the leading contribution in defining the cation distribution (Sarkar et al., 2022).

Another point which is usually disregarded in HEO research is that, in applications where chemical reactivity is concerned—catalysis (Chen et al., 2018; Xu et al., 2020; Albedwawi et al., 2021; Tavani et al., 2021), electrochemistry (Sarkar et al., 2018b, 2019; Nguyen et al., 2021; Zhang et al., 2021; Callegari et al., 2022), batteries (Wang et al., 2019; Zhao et al., 2020; Chen et al., 2021), etc.—the quest for stability is not a major concern. In other words, the additional stabilizing contribution due to configurational entropy may even be *detrimental* in these cases.

The aim of this paper is to contribute to a better understanding of the role of configurational entropy in the application of rock-salt HEOs as anode materials in lithium batteries. The starting point of this investigation is our previous mechanistic work on the lithiation of the $Mg_{0.2}Co_{0.2}Ni_{0.2}Cu_{0.2}Zn_{0.2}O$ oxide (HEO), where we showed that the reaction proceeds via a complex and irreversible conversion mechanism, leading to a final collapse of the HEO rock-salt structure (Ghigna et al., 2020; Tavani et al., 2020). We thus synthesized a series of high and medium entropy oxides (HEOs and MEOs), whose performance as anodic materials were tested. Here, high entropy oxides are defined as having S_{config} of at least 1.61R while, for medium entropy oxides, we intend solid solutions having S_{config} between 0.9 and 1.6R.

In this paper, only ternary and quaternary compounds, in addition to the quinary HEO, are investigated. Concerning the use of the corresponding parent oxides as anodes for Li-ion batteries, binary oxides such as ZnO, CoO, CuO and NiO have already been widely discussed in several reviews (see, for instance, Reddy et al., 2013). For oxides with a rock-salt structure (MO; M = Co, Ni), the electrochemical reaction during Li cycling occurs through the conversion mechanism, involving the formation and decomposition of Li_2O and the consequent reduction/oxidation of metal nanoparticles. ZnO has been deeply investigated for Li storage behavior via an alloying-dealloying mechanism, due to the Zn affinity to form alloys with Li at potential below 1.0 V with consequent high capacity (Reddy et al., 2013; Quartarone et al., 2016). MgO, on the contrary, is poorly active (Ghigna et al., 2020) and its usage as a negative electrode in Li ion batteries should not be taken into account.

The main conclusions of the present work are: i) the reduction potential of the five-component HEO is higher than those of the four- and three-component MEOs; ii) the capacity of the materials generally increases as S_{config} increases. Both these effects are discussed in terms of the thermodynamics of the systems.

Experimental

Synthesis

All samples were obtained via solid-state synthesis, starting with high-purity reagents (purity >99.7%) from Sigma Aldrich (CoO, NiO, ZnO, MgO, CuO). In all cases, the oxides were weighted in stoichiometric proportion and ground with an agate mortar and pestle. The resulting powder was pressed uniaxially into pellets and then calcinated at 1,200°C (ramp rate 5°C/min) for six hours and quenched in air to room temperature. After that, single-phase rock salt oxides with micrometric size were obtained with an additional treatment at 1,000°C for six hours (ramp rate 5°C/min).

Anode preparation and cell assembly

The anode slurry was prepared by using 70 wt% of active material (MEO-3, MEO-4, HEO-5), 20% of conductive carbon black (Timcal-Imerys, Super C65) and 10% of a binder (polyvinylidene fluoride, PVDF). The solid content of all slurries was kept between 26 wt% and 28 wt%. The materials and carbon powders were twice mixed in zirconia jars by a planetary ball mill at 150 rpm for ten minutes, with a rest period of five minutes. The polymeric binder was subsequently added and mixed using a similar procedure. The as-prepared mixture was dispersed in N-methylpyrrolidone (NMP) to obtain the slurry, which was cast on a copper foil using a doctor blade with a wet thickness of 300 μm.

The cast slurry was dried under vacuum at 80°C to avoid moisture and oxygen contamination. The anode (active mass~ 2 mg cm^{-2}) was finally cut into 2 cm^2 disks and stored in a glove box (MBraum, O_2, H_2O < 0.5 ppm) before electrochemical measurement. All the functional tests were performed using a coin cell type (CR2032 - MTI Corp.) assembled in an Ar-filled glove box (H_2O and O_2 < 0.5 ppm). Metallic Li was used as counter electrode. Electrodes were separated with a Whatman glass fiber separator, imbibed by 120 µL of liquid electrolyte, consisting of a solution of 1 M $LiPF_6$ in ethylene carbonate: dimethyl carbonate (LP30, EC:DMC, 50:50 vol.%) (Sigma-Aldrich).

Characterization

X-ray powder diffraction was performed using a Bruker D8 Advance diffractometer in Bragg-Brentano geometry equipped with a Ni-filtered Cu-Kα radiation. The diffraction patterns of the powder samples were collected in the 10–90° 2θ range, with 0.02° of step. Post-mortem XRD on the composite anodes, stuck onto a glass holder for the purpose, were collected in the 15–80° 2θ range, with 0.04° of step.

Transmission electron microscopy (TEM) and high resolution (HR) TEM analyses were carried out by a side-entry JEOL 3010-UHR microscope operating at 300 kV, equipped with a LaB_6 filament, (2k × 2k)-pixel Gatan US1000 CCD camera and an Oxford INCA EDS instrument for atomic recognition via energy dispersive spectroscopy (EDS). The samples, in the form of powders, were briefly contacted by an Au grid with a lacey carbon film, which resulted in electrostatic adhesion of the particles to the sample holder.

The size distribution and mean diameter (d_m) of the crystalline nanoparticles were obtained by considering a statistically representative number of nanoparticles (>120 for each sample) on different HRTEM images. The d_m was calculated using the following equation:

$$d_m = \sum d_i \cdot n_i / \sum n_i$$

where n_i is the number of particles of diameter d_i.

Moreover, a detailed structural characterization of the MEOs and HEO within the carbon matrix was obtained by measuring the distances among the spots due to the diffracted beam and the transmitted beam in the corresponding Fourier transform (FT) images of all HR-TEM micrographs collected on different regions of the Au grid. At least 100 spots were measured for each sample.

The electrochemical characterization of the anodes was performed using potentio-electrochemical impedance spectroscopy (PEIS) and galvanostatic cycling with potential limitation (GCPL) on Li/HEO cells in a voltage range between 0.01 and 3.0 V at room temperature and different C rates by means of a battery tester (Bio-Logic BCS-810).

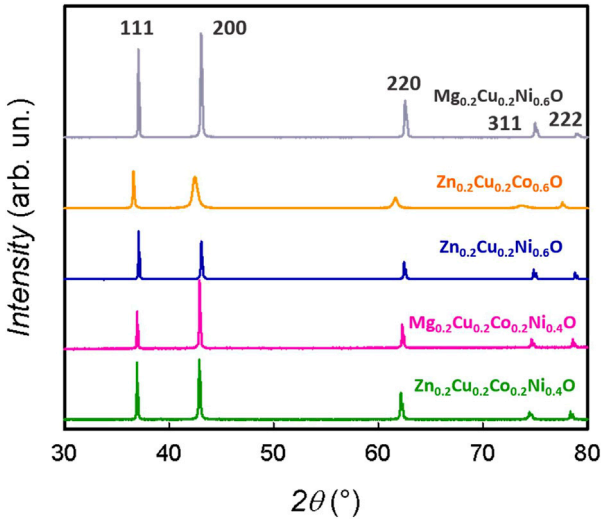

FIGURE 1
X-ray diffraction patterns for all the medium-entropy oxide compositions. The patterns are indexed according to the rock-salt structure (*Fm*$\bar{3}$m, nr. 225).

Results

MEOs were synthetized through conventional solid-state synthesis. The compositions investigated were $Zn_{0.2}Cu_{0.2}Co_{0.2}Ni_{0.4}O$, $Mg_{0.2}Cu_{0.2}Co_{0.2}Ni_{0.4}O$, $Zn_{0.2}Cu_{0.2}Ni_{0.6}O$, $Zn_{0.2}Cu_{0.2}Co_{0.6}O$, $Mg_{0.2}Cu_{0.2}Ni_{0.6}O$, while the electrochemical mechanism of $Cu_{0.2}Zn_{0.2}Mg_{0.2}Co_{0.2}Ni_{0.2}O$ had already been evaluated in a previous work (Ghigna et al., 2020). All materials bear a relationship with the prototypical quinary high entropy oxide, $Cu_{0.2}Zn_{0.2}Mg_{0.2}Co_{0.2}Ni_{0.2}O$. As already reported in Fracchia et al. (2022), as long as the molar fractions of Cu^{2+} and Zn^{2+} are kept below 0.2, then XRPD and HR-TEM imaging, coupled to EDS analysis, could demonstrate that pure single-phase oxides can be obtained even by progressively removing the number of components. As a general rationale, Cu^{2+} was included in all samples, being the major factor responsible for the electrochemical activity of $Cu_{0.2}Zn_{0.2}Mg_{0.2}Co_{0.2}Ni_{0.2}O$ and the first metal to be reduced, according to its standard reduction potential and to a previous study (Ghigna et al., 2020). Co^{2+} and Ni^{2+} are expected to give a similar contribution, being both electrochemically active (they are promptly reduced after Cu^{2+} to the metallic state during lithiation) while contributing to the stabilization of the rock-salt matrix. As a result, all specimens contain either Ni^{2+} or Co^{2+} in variable proportion.

Finally, the role of Zn^{2+} and Mg^{2+} in the lithiation/delithiation process has not been completely assessed. According to Sarkar et al. (2018b), Mg does not contribute directly to the conversion reaction but favors the preservation of the rock-salt phase. Similarly, Chen et al. (Qiu et al., 2019) suggested that Zn^{2+} is involved in the formation of an alloy with

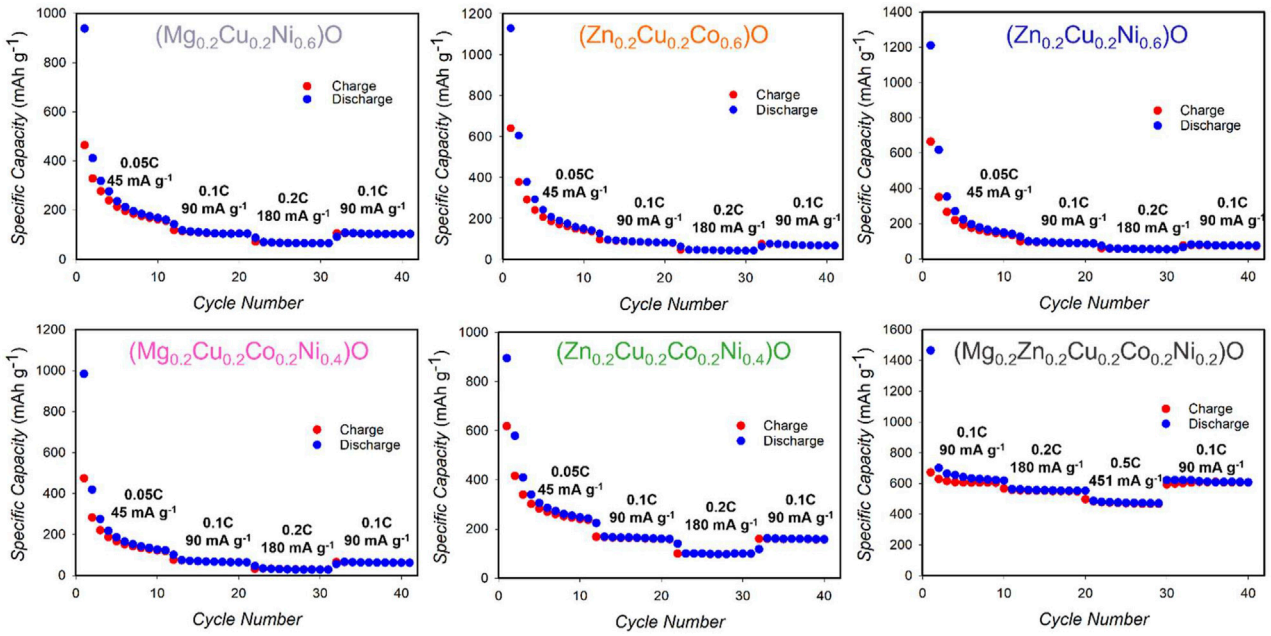

FIGURE 2
Rate performances of MEO 3, MEO 4 and HEO-5 anodes cycled from 0.01 to 3.0 V at different current densities.

Li, while Mg^{2+} does not directly contribute to the reaction, instead forming MgO, which remains inactive throughout the lithiation/delithiation process. In our previous work (Ghigna et al., 2020), however, we found evidence of a complex mechanism involving both Zn^{2+} and Mg^{2+} in the formation of Li alloys. Taking this into account, quaternary and ternary samples either contained Zn^{2+} *or* Mg^{2+} in order to separate their contribution. This approach had the twofold scope of i) evaluating the role of configurational entropy by progressively decreasing it from quinary to ternary compounds, and ii) gaining a better insight into the role of Zn^{2+} and Mg^{2+}.

The X-ray diffraction patterns for all compositions, reported in Figure 1, confirm the formation of pure single-phase oxides where all reflections can be indexed according to the rock-salt phase (space group $Fm\bar{3}m$, nr. 225). In the case of $Zn_{0.2}Cu_{0.2}Co_{0.6}O$, all peaks apart from those related to the *hhh* family show a notable broadening. This effect was already in evidence in previous works (Berardan et al., 2017; Fracchia et al., 2020a) and is due to a deviation from the ideal cubic structure, possibly an incipient tetragonal distortion, driven by the strong Jahn-Teller effect of Cu^{2+} in the d^9 electronic configuration.

When tested as anodes for Li batteries, the samples studied in this work display a remarkable variety of performances. We first discuss the reversible capacity, which in our previous work was demonstrated to be due to i) reduction of MO to M and Li_2O and (ii) formation of Li/M alloys (M = Zn, Mg). For the HEO-5 at 0.1 C, the theoretical capacity amounts to 600–615 $mAhg^{-1}$, of which 197 $mAhg^{-1}$ are due to the above reactions when M = Zn, and 418 $mAhg^{-1}$ when M = Mg (Ghigna et al., 2020). These values allow calculation of the reversible capacities of the different samples investigated in this work, shown in Figure 2 as a function of the number of cycles of lithiation/delithiation.

The $(Zn_{0.2}Cu_{0.2}Co_{0.2}Ni_{0.4})O$ sample shows a capacity close to the theoretical value, a good stability in the subsequent lithiation/delithiation processes, which is demonstrated by the capacity values obtained during the recovery (31–40 cycles). The $(Mg_{0.2}Cu_{0.2}Co_{0.2}Ni_{0.4})O$ sample, on the contrary, shows very poor electrochemical performances, with a reversible capacity which amounts to only *ca.* 1/6 of its theoretical value.

The three three-component samples, $(Zn_{0.2}Cu_{0.2}Ni_{0.6})O$, $(Zn_{0.2}Cu_{0.2}Co_{0.6})O$, and $(Mg_{0.2}Cu_{0.2}Ni_{0.6})O$, all have capacities well below the calculated values, amounting to ½, ½ and ¼ of the theoretical.

The capacity values of Figure 2 allow assessment of the performances of the different oxides studied in this work. However, the lithiation/delithiation experiments are also helpful in addressing some important aspects involving the stability of the solid solutions.

With this aim, we plotted in Figure 3 the potential curves of the various oxides described in this work as a function of the specific capacity. The potentials in Figure 3A refer to the first discharge semi-cycle (lithiation) and, therefore, to a reduction reaction. It is clearly apparent from the plots that, in every case, the lithiation proceeds through a complex reaction chain involving several steps.

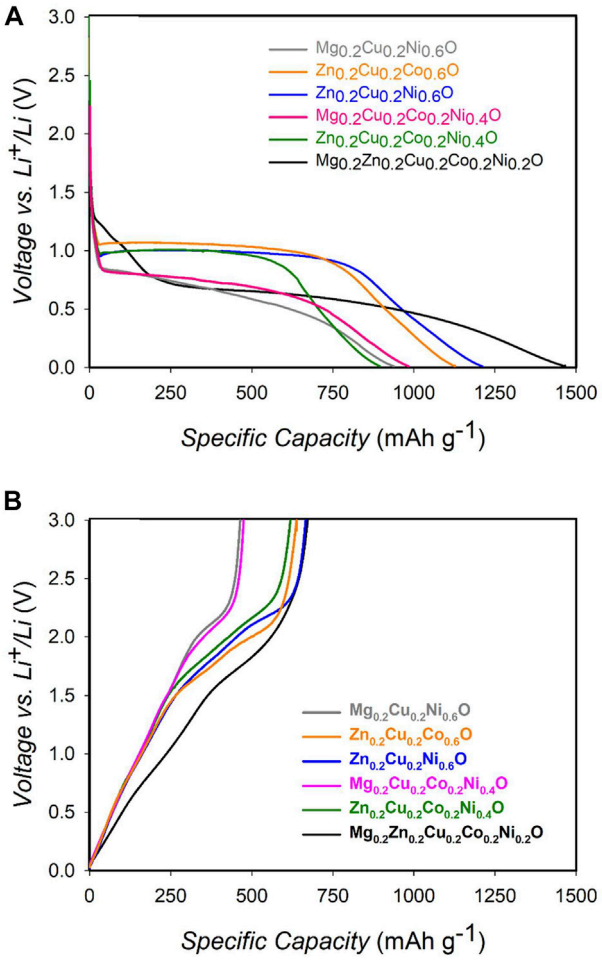

FIGURE 3
Voltage profile of HEO 3, HEO 4 and HEO-5 for the first lithiation **(A)** and de-lithiation **(B)** step/process.

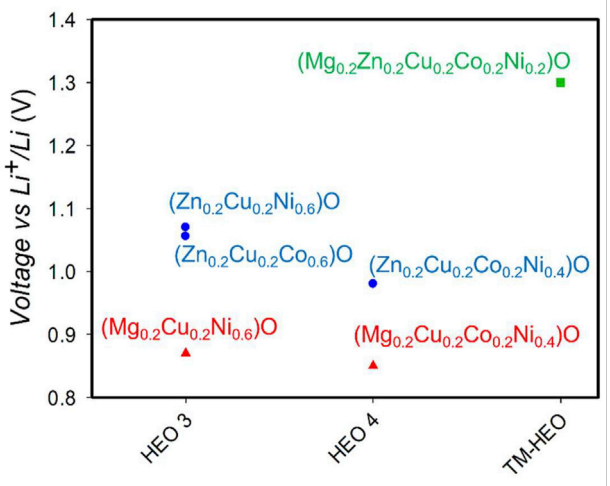

FIGURE 4
Onset potentials of the first lithiation step for the different HEO anodes.

In addition, for the delithiation process, the presence of small differences in the voltage profile for the different materials can be attributed to the complex mechanism of lithiation, where different cations react at different potentials. In summary, the difference in the potential for the onset and working values can be attributed to the reaction mechanisms in both cases.

We here focus on the first phenomenon of the lithiation process, which, for HEO-5, takes place at *ca.* 1.3 V. It should be noted that this first reaction step refers to the reduction of structural Cu(II) according to the partial reactions (Ghigna et al., 2020):

$$2CuO + 2Li \rightarrow Cu_2O + Li_2O$$
$$Cu_2O + 2Li \rightarrow 2Cu + Li_2O$$

After these reactions, Cu exits the HEO-5 and is segregated as metallic Cu. Therefore, the Gibbs free energy of these reactions can be used as a measure of the stability of Cu(II) in HEO-5 and, therefore, of HEO-5 itself. Via the equation $\Delta G = -nF\Delta E$, the Gibbs free energy of reaction is measured by the potential. From the data in Figure 3, it is clearly apparent that the potential at which the first lithiation reaction takes place depends on the actual composition of the sample. To make this point clearer, Figure 4 plots the onset potentials of the first lithiation step as a function of the number of components in the materials. Figure 4 clearly demonstrates a complex behavior, which is the result of several different phenomena occurring. Here, we only note that at least two competing effects are evident:

1) Removing Zn from the solid solutions decreases the potentials. It is difficult to rationalize this effect by simple thermodynamic arguments based on ideal mixing because, in ideal mixtures, the components are, in principle, indistinguishable. Therefore, this indicates a possible cooperative role of Zn and Cu in the stabilization of the HEO-5 structure.
2) Neglecting this possible cooperative effect of Zn and Cu, an overall tendency for the potential to increase with increasing number of components can be noticed. This effect is expected as it reflects the stabilizing contribution of configurational entropy;

The complexity of the lithiation process is also testified by the XRD patterns of the samples at the end of the 40th cycle, shown in Figure 5. All the samples show, although to a different extent, a loss of crystallinity, which is analogous with what is found for the HEO-5 quinary solid solution (Qiu et al., 2019; Ghigna et al., 2020; Wang et al., 2021). In this case, the amorphization is greater for the samples containing Zn and smaller for the series containing Mg. In these last two cases, in addition to the

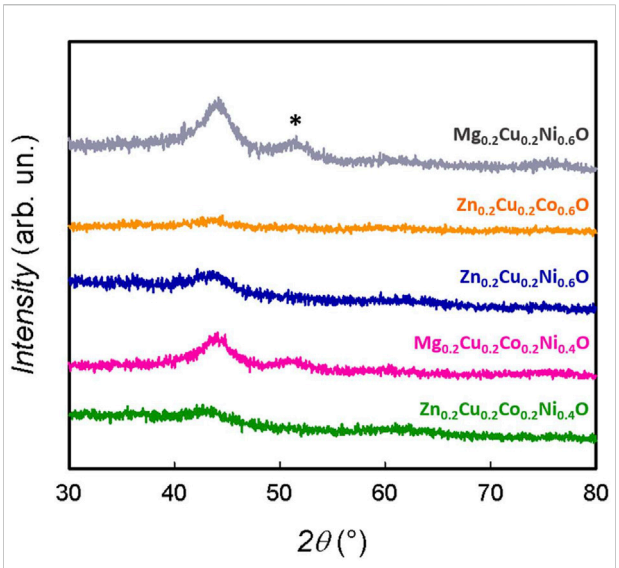

FIGURE 5
X-ray diffraction patterns of the electrodes after use. The asterisk indicates the 200 reflection attributed to a metallic phase with the *fcc* structure.

principal peak at *ca.* 44°—the 200 reflection of an oxide with the rock-salt structure —a broad diffraction effect at ca. 50° is apparent (marked by an asterisk in the figure). This can be attributed to the 200 reflection of a metal with the *fcc* structure (e.g. Cu or Ni). It should be noted that the 111 reflection of these metals falls around 44°, thus probably overlapping with the rock-salt signal.

To investigate possible morphological and structural changes induced by the electrochemical cycles in the Li ion batteries, HRTEM analyses were carried out on both $Zn_{0.2}Cu_{0.2}Ni_{0.6}O$ and $Mg_{0.2}Cu_{0.2}Co_{0.2}Ni_{0.4}O$ containing electrodes after use (the results are shown in Figure 6).

In both cases, the observation of the electrodes after use reveals the presence of carbon-rich zones due to the carbon matrix (highlighted with dashed ovals: Figures 6A,D) and of small crystalline nanoparticles. In particular, the $Zn_{0.2}Cu_{0.2}Ni_{0.6}O$-containing electrode has nanoparticles of a quite homogeneous size, as revealed by the size distribution reported in Figure 6C, which resulted in an average size of 2.9 ± 0.4 nm. In agreement with the XRD findings, the analysis of the Fourier transform (FT) of the images (Figure 7) showed the presence of points corresponding to the (111) and (200) planes of the rock-salt cubic phase with 48% and 33% relative abundance respectively, indicating that the electrochemical performance did not alter the overall crystallinity of the MEO. In addition, diffraction spots (11%) are apparent, due to the (002) plane of hexagonal graphite (d = 3.38 Å) contained in the carbon matrix of the electrode. Moreover, the spots related to the (002) plane of a *fcc* cubic metal were detected in 11% relative abundance, along with the (111) plane of cubic NiO (2% relative abundance) and the (111) plane of monoclinic CuO (2% relative abundance). It is worth nothing that the contribution by the (111) plane (d = 2.04 Å) of the *fcc* metal overlaps with that of the 200 plane of the rock salt cubic phase (d = 2.104 Å); moreover, the presence of cubic metallic Cu cannot be excluded.

Conversely, the MEO nanoparticle size distribution obtained for the $Mg_{0.2}Cu_{0.2}Co_{0.2}Ni_{0.4}O$-containing electrode (Figure 6E) is broader than that of the $Zn_{0.2}Cu_{0.2}Ni_{0.6}O$-containing electrode (Figure 6C), resulting in a slightly higher average size (3.3 ± 0.7 nm). Besides the presence of almost the same diffraction spots observed for the $Zn_{0.2}Cu_{0.2}Ni_{0.6}O$-containing electrode, the main difference is ascribed to their different relative abundance. In more detail, 22% and 52% amounts were obtained for the (111) and (200) planes of the rocksalt cubic phase, respectively. The relative abundance of the spot related to the (200) plane of the *fcc* metal is 9%, whereas the presence of the 002 plane of hexagonal graphite is very similar in both materials (13% vs. 11% obtained for the $Zn_{0.2}Cu_{0.2}Ni_{0.6}O$-containing electrode). In addition, the spot associated with the (111) plane of cubic CoO reached 4% relative abundance. As with before, the presence of metallic Cu cannot be excluded.

Besides the additional presence of the NiO and CuO crystalline phases in the $Zn_{0.2}Cu_{0.2}Ni_{0.6}O$-containing electrode and of the CoO phase in the $Mg_{0.2}Cu_{0.2}Co_{0.2}Ni_{0.4}O$-containing electrode, two main observations can be made: i) the (111) and (200) planes of the rock-salt cubic phase have different relative abundance in the two samples; ii) the relative amount of the spots related to the (200) plane of the *fcc* metal is larger in the $Mg_{0.2}Cu_{0.2}Co_{0.2}Ni_{0.4}O$-containing electrode than in the $Zn_{0.2}Cu_{0.2}Ni_{0.6}O$-containing electrode (9% vs. 4%). Such features seem to reveal the occurrence of different structural changes in the two materials upon electrochemical tests.

Discussion and conclusion

In this work, we investigated the role of configurational entropy in the electrochemical performances of MEO-3,4 and HEO-5. Our approach consisted of decreasing the stabilizing effect of configurational entropy by preparing solid solutions with less-than-five components and testing them as anodes in lithium batteries, and then comparing the performances against the five component HEO-5. Furthermore, we here note that several contributions add to the Gibbs free energy of the HEO-5 cubic rock salt structure, in addition to the stabilizing term given by the configurational entropy of mixing. Concerning the solubility of CuO, because CuO is stable in a monoclinic structure, the enthalpy of the phase transition of CuO from the monoclinic to the rock-salt structure needs to be taken into account. A similar argument applies to ZnO, which is stable in a wurtzite-related crystal structure. In order to keep these

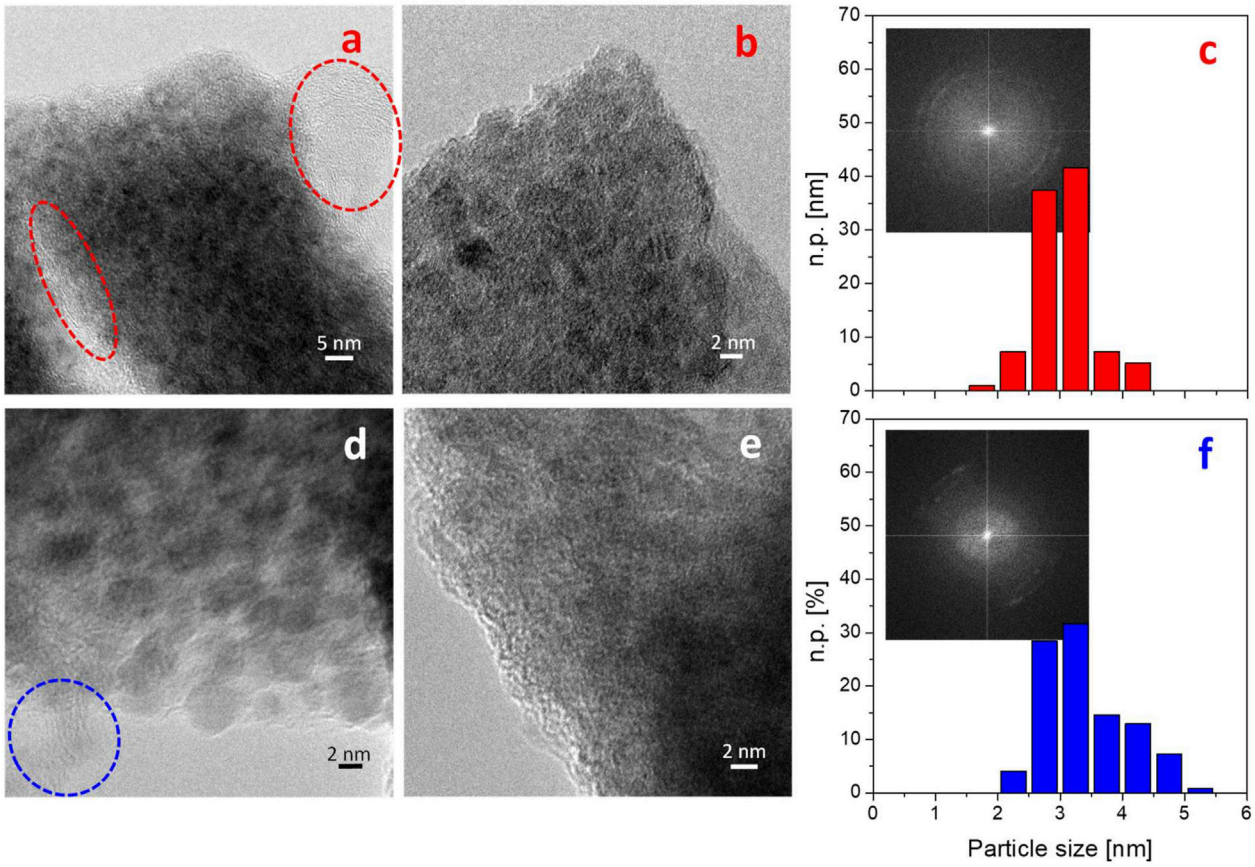

FIGURE 6
Representative TEM **(A,D)** and HRTEM **(B,E)** images and particle size distributions **(C,F)** of $Zn_{0.2}Cu_{0.2}Ni_{0.6}O$ (upper panels) and $Mg_{0.2}Cu_{0.2}Co_{0.2}Ni_{0.4}O$ (lower panels) containing electrodes after use. The FT of the images in **(B,E)** are shown as insets in panels **(C,F)**, respectively. Dashed ovals highlight zones with lower contrast and a typical layered structure of carbon black employed to prepare the anode. Instrumental magnification: ×300000 **(A)** and 600000× **(B,D,E)**.

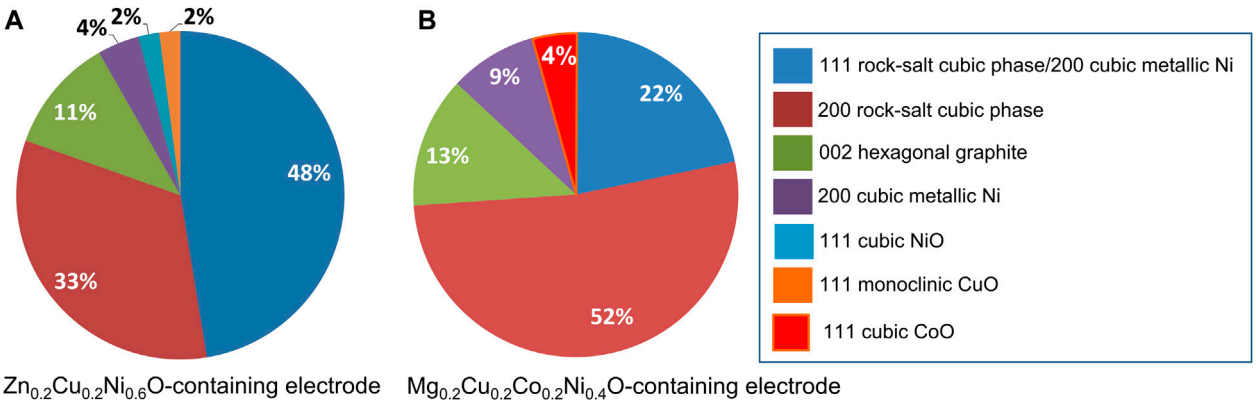

FIGURE 7
Relative abundance of the diffraction spots measured on the FT images obtained from the HRTEM images of $Zn_{0.2}Cu_{0.2}Ni_{0.6}O$ **(A)** and $Mg_{0.2}Cu_{0.2}Co_{0.2}Ni_{0.4}O$ **(B)** containing electrodes after use.

contributions constant across the series of samples, we kept the global molar fraction of parent oxides with the rock-salt structure constant at 0.6. Our results unambiguously show that the role of configurational entropy is twofold. On one hand, the stabilizing effect of S_{config} in the Gibbs free energy is very apparent in the reduction potential of the five component HEO-5, which is higher than those of the four and three component solid solutions. Considering that the configurational entropy enters the Gibbs free energy trough the relation $\Delta G = \Delta H - T\Delta S$ and that, in turn, the Gibbs free energy of the reaction is related to the potential trough $\Delta G = -nF\Delta E$, it is apparent that increasing the configurational entropy gives more negative values for ΔG and therefore increases the potential. On the other hand, S_{config} has also a beneficial effect in determining the specific capacity of the solid solutions: on average, the higher the S_{config}, the higher the capacity. It is more difficult to rationalize this effect: it is contrary to what would be initially expected. The specific capacity is an assessment of the reactivity of the samples, and it should be therefore decreased by an increased stability. This is equivalent to a state in which, where reactivity is concerned, the quest for stability is detrimental. However, some additional considerations are due in this respect. Firstly, we note that all the solid solutions are *metastable* at room temperature, and not stable, as they tend to segregate CuO and distort into a tetragonal structure upon heating, and that both these effects are facilitated by increasing the number of components (Fracchia et al., 2022). Another point to note is that the conversion reaction leads to significant amorphization, with a significant degree of irreversibility also detected.

A rationale of this intricate behavior can start with the following premises. All the solid solutions are apparently near the edge of a stability limit, as it is proven by their metastability. The higher the number of components, the closer the stability limit. This affects both the amorphization and the irreversibility of the conversion reaction. Indeed, on average, the samples after the reaction are found to be less crystalline when the number of components is higher.

Data availability statement

The original contributions presented in the study are included in the article/supplementary material, and further inquiries can be directed to the corresponding author.

Author contributions

All authors listed have made a substantial, direct, and intellectual contribution to the work and approved it for publication.

Conflict of interest

The authors declare that the research was conducted in the absence of any commercial or financial relationships that could be construed as a potential conflict of interest.

Publisher's note

All claims expressed in this article are solely those of the authors and do not necessarily represent those of their affiliated organizations, or those of the publisher, the editors and the reviewers. Any product that may be evaluated in this article, or claim that may be made by its manufacturer, is not guaranteed or endorsed by the publisher.

References

Albedwawi, S. H., AlJaberi, A., Haidemenopoulos, G. N., and Polychronopoulou, K. (2021). High entropy oxides-exploring a paradigm of promising catalysts: A review. *Mat. Des.* 202, 109534. doi:10.1016/j.matdes.2021.109534

Berardan, D., Meena, A. K., Franger, S., Herrero, C., and Dragoe, N. (2017). Controlled Jahn-Teller distortion in (MgCoNiCuZn)O-based high entropy oxides. *J. Alloys Compd.* 704, 693–700. doi:10.1016/j.jallcom.2017.02.070

Bulazirk, J., Davies, P. K., and Navrotsky, A. (1986). Thermodynamics of solid-solution formation in NiO-CuO. *J. Am. Ceram. Soc.* 69, 453–457. doi:10.1111/j.1151-2916.1986.tb07444.x

Callegari, D., Coduri, M., Fracchia, M., Ghigna, P., Braglia, L., Anselmi Tamburini, U., et al. (2022). Lithium intercalation mechanisms and critical role of multi-doping in $LiFe_xMn_{2-x-y}Ti_yO_4$ as high-capacity cathode material for lithium-ion batteries. *J. Mat. Chem. C Mat.* 10, 8994–9008. doi:10.1039/d2tc00573e

Chen, H., Fu, J., Zhang, P., Peng, H., Abney, C. W., Jie, K., et al. (2018). Entropy-stabilized metal oxide solid solutions as CO oxidation catalysts with high-temperature stability. *J. Mat. Chem. A* 6, 11129–11133. doi:10.1039/c8ta01772g

Chen, H., Qiu, N., Wu, B., Yang, Z., Sun, S., Wang, Y., et al. (2020). A new spinel high-entropy oxide (Mg0.2Ti0.2Zn0.2Cu0.2Fe0.2)3O4 with fast reaction kinetics and excellent stability as an anode material for lithium ion batteries. *RSC Adv.* 10, 9736–9744. doi:10.1039/d0ra00255k

Chen, Y., Fu, H., Huang, Y., Huang, L., Zheng, X., Dai, Y., et al. (2021). Opportunities for high-entropy materials in rechargeable batteries. *ACS Mat. Lett.* 3, 160–170. doi:10.1021/acsmaterialslett.0c00484

Dąbrowa, J., Stygar, M., Mikuła, A., Knapik, A., Mroczka, K., Tejchman, W., et al. (2018). Synthesis and microstructure of the (Co, Cr, Fe, Mn, Ni)3O4 high entropy oxide characterized by spinel structure. *Mat. Lett.* 216, 32–36. doi:10.1016/j.matlet.2017.12.148

Davies, P. K. (1982). An X-ray powder diffraction study of phases in the system CuO - NiO - MgO at 1000°C. *J. Electrochem. Soc.* 129, 31C–35C. doi:10.1149/1.2123819

Fracchia, M., Coduri, M., Manzoli, M., Ghigna, P., and Anselmi Tamburini, U. (2022). Is configurational entropy the main stabilizing term in rock-salt $Mg_{0.2}Co_{0.2}Ni_{0.2}Cu_{0.2}Zn_{0.2}O$ high-entropy oxide? *Nat. Commun.* 13, 2977. doi:10.1038/s41467-022-30674-0

Fracchia, M., Ghigna, P., Pozzi, T., Anselmi Tamburini, U., Colombo, V., Braglia, L., et al. (2020a). Stabilization by configurational entropy of the Cu(II) active site during CO oxidation on Mg 0.2 Co 0.2 Ni 0.2 Cu 0.2 Zn 0.2 O. *J. Phys. Chem. Lett.* 11, 3589–3593. doi:10.1021/acs.jpclett.0c00602

Fracchia, M., Manzoli, M., Anselmi-Tamburini, U., and Ghigna, P. (2020b). A new eight-cation inverse high entropy spinel with large configurational entropy in both

tetrahedral and octahedral sites: Synthesis and cation distribution by X-ray absorption spectroscopy. *Scr. Mat.* 188, 26–31. doi:10.1016/j.scriptamat.2020.07.002

George, E. P., Raabe, D., and Ritchie, R. O. (2019). High-entropy alloys. *Nat. Rev. Mat.* 4, 515–534. doi:10.1038/s41578-019-0121-4

Ghigna, P., Airoldi, L., Fracchia, M., Callegari, D., Anselmi-Tamburini, U., D'angelo, P., et al. (2020). Lithiation mechanism in high-entropy oxides as anode materials for Li-ion batteries: An operando XAS study. *ACS Appl. Mat. Interfaces* 12, 50344–50354. doi:10.1021/acsami.0c13161

Gild, J., Samiee, M., Braun, J. L., Harrington, T., Vega, H., Hopkins, P. E., et al. (2018). High-entropy fluorite oxides. *J. Eur. Ceram. Soc.* 38, 3578–3584. doi:10.1016/j.jeurceramsoc.2018.04.010

Jiang, S., Hu, T., Gild, J., Zhou, N., Nie, J., Qin, M., et al. (2018). A new class of high-entropy perovskite oxides. *Scr. Mat.* 142, 116–120. doi:10.1016/j.scriptamat.2017.08.040

Mao, A., Xie, H. X., Xiang, H. Z., Zhang, Z. G., Zhang, H., Ran, S., et al. (2020). A novel six-component spinel-structure high-entropy oxide with ferrimagnetic property. *J. Magn. Magn. Mat.* 503, 166594. doi:10.1016/j.jmmm.2020.166594

Miracle, D. B., and Senkov, O. N. (2017). A critical review of high entropy alloys and related concepts. *Acta Mat.* 122, 448–511. doi:10.1016/j.actamat.2016.08.081

Navrotsky, A., and Muan, A. (1971). Activity-Composition relations in the systems CoO-ZnO and NiO-ZnO at 1050 °C. *J. Inorg. Nucl. Chem.* 33, 35–47. doi:10.1016/0022-1902(71)80006-4

Nguyen, T. X., Liao, Y. C., Lin, C. C., Su, Y. H., and Ting, J. M. (2021). Advanced high entropy perovskite oxide electrocatalyst for oxygen evolution reaction. *Adv. Funct. Mat.* 31, 2101632. doi:10.1002/adfm.202101632

Qiu, N., Chen, H., Yang, Z., Sun, S., Wang, Y., Cui, Y., et al. (2019). A high entropy oxide (Mg0.2Co0.2Ni0.2Cu0.2Zn0.2O) with superior lithium storage performance. *J. Alloys Compd.* 777, 767–774. doi:10.1016/j.jallcom.2018.11.049

Quartarone, E., Dall'Asta, V., Resmini, A., Tealdi, C., Tredici, I. G., Anselmi Tamburini, U., et al. (2016). P. Graphite-coated ZnO nanosheets as high-capacity, highly stable, and binder-free anodes for lithium-ion batteries. *J. Power Sources* 320, 314–321. doi:10.1016/j.jpowsour.2016.04.107

Reddy, M. V., Subba Rao, G. V., and Chowdari, B. V. R. (2013). Metal oxides and oxysalts as anode materials for Li ion batteries. *Chem. Rev. 2013* 113 (7), 5364–5457. doi:10.1021/cr3001884

Rost, C. M., Sachet, E., Borman, T., Moballegh, A., Dickey, E. C., Hou, D., et al. (2015). Entropy-stabilized oxides. *Nat. Commun.* 6, 8485. doi:10.1038/ncomms9485

Sarkar, A., Djenadic, R., Wang, D., Hein, C., Kautenburger, R., Clemens, O., et al. (2018a). Rare Earth and transition metal based entropy stabilised perovskite type oxides. *J. Eur. Ceram. Soc.* 38, 2318–2327. doi:10.1016/j.jeurceramsoc.2017.12.058

Sarkar, A., Eggert, B., Witte, R., Lill, J., Velasco, L., Wang, Q., et al. (2022). Comprehensive investigation of crystallographic, spin-electronic and magnetic structure of (Co0.2Cr0.2Fe0.2Mn0.2Ni0.2)3O4: Unraveling the suppression of configuration entropy in high entropy oxides. *Acta Mat.* 226, 117581. doi:10.1016/j.actamat.2021.117581

Sarkar, A., Velasco, L., Wang, D., Wang, Q., Talasila, G., de Biasi, L., et al. (2018b). High entropy oxides for reversible energy storage. *Nat. Commun.* 9, 3400. doi:10.1038/s41467-018-05774-5

Sarkar, A., Wang, Q., Schiele, A., Chellali, M. R., Bhattacharya, S. S., Wang, D., et al. (2019). High-entropy oxides: Fundamental aspects and electrochemical properties. *Adv. Mat.* 31, 1806236. doi:10.1002/adma.201806236

Spiridigliozzi, L., Ferone, C., Cioffi, R., and Dell'Agli, G. (2021). A simple and effective predictor to design novel fluorite-structured High Entropy Oxides (HEOs). *Acta Mat.* 202, 181–189. doi:10.1016/j.actamat.2020.10.061

Stygar, M., Dąbrowa, J., Moździerz, M., Zajusz, M., Skubida, W., Mroczka, K., et al. (2020). Formation and properties of high entropy oxides in Co-Cr-Fe-Mg-Mn-Ni-O system: Novel (Cr, Fe, Mg, Mn, Ni)3O4 and (Co, Cr, Fe, Mg, Mn) 3O4 high entropy spinels. *J. Eur. Ceram. Soc.* 40, 1644–1650. doi:10.1016/j.jeurceramsoc.2019.11.030

Tavani, F., Fracchia, M., Pianta, N., Ghigna, P., Quartarone, E., D'Angelo, P., et al. (2020). Multivariate curve resolution analysis of operando XAS data for the investigation of the lithiation mechanisms in high entropy oxides. *Chem. Phys. Lett.* 760, 137968. doi:10.1016/j.cplett.2020.137968

Tavani, F., Fracchia, M., Tofoni, A., Braglia, L., Jouve, A., Morandi, S., et al. (2021). Structural and mechanistic insights into low-temperature CO oxidation over a prototypical high entropy oxide by Cu L-edge operando soft X-ray absorption spectroscopy. *Phys. Chem. Chem. Phys.* 23, 26575–26584. doi:10.1039/d1cp03946f

Tsai, M., Yeh, J., Tsai, M., and Yeh, J. (2014). High-entropy alloys : A critical review. *Mat. Res. Lett.* 2, 107–123. doi:10.1080/21663831.2014.912690

Vinnik, D. A., Trofimov, E. A., Zhivulin, V. E., Gudkova, S. A., Zaitseva, O. V., Zherebtsov, D. A., et al. (2020). High entropy oxide phases with perovskite structure. *Nanomaterials* 10, 268. doi:10.3390/nano10020268

Wang, Q., Sarkar, A., Li, Z., Lu, Y., Velasco, L., Bhattacharya, S. S., et al. (2019). High entropy oxides as anode material for Li-ion battery applications: A practical approach. *Electrochem. Commun.* 100, 121–125. doi:10.1016/j.elecom.2019.02.001

Wang, S. Y., Chen, T. Y., Kuo, C. H., Lin, C. C., Huang, S. C., Lin, M. H., et al. (2021). Operando synchrotron transmission X-ray microscopy study on (Mg, Co, Ni, Cu, Zn)O high-entropy oxide anodes for lithium-ion batteries. *Mat. Chem. Phys.* 274, 125105. doi:10.1016/j.matchemphys.2021.125105

Xu, H., Zhang, Z., Liu, J., Do-Thanh, C. L., Chen, H., Xu, S., et al. (2020). Entropy-stabilized single-atom Pd catalysts via high-entropy fluorite oxide supports. *Nat. Commun.* 11, 3908. doi:10.1038/s41467-020-17738-9

Yan, X., Constantin, L., Lu, Y., Silvain, J. F., Nastasi, M., Cui, B., et al. (2018). Hf0.2Zr0.2Ta0.2Nb0.2Ti0.2)C high-entropy ceramics with low thermal conductivity. *J. Am. Ceram. Soc.* 101, 4486–4491. doi:10.1111/jace.15779

Zabdyr, L. A., and Fabrichnaya, O. B. (2002). Phase equilibria in the cobalt oxide-copper oxide system. *J. Phase Equilibria* 23, 149–155. doi:10.1361/1054971023604161

Zhang, Y., Dai, W., Zhang, P., Lu, T., and Pan, Y. (2021). *In-situ* electrochemical tuning of (CoNiMnZnFe)3O3.2 high-entropy oxide for efficient oxygen evolution reactions. *J. Alloys Compd.* 868, 159064. doi:10.1016/j.jallcom.2021.159064

Zhao, C., Ding, F., Lu, Y., Chen, L., and Hu, Y. S. (2020). High-entropy layered oxide cathodes for sodium-ion batteries. *Angew. Chem. Int. Ed.* 59, 264–269. doi:10.1002/anie.201912171